

1 **Historical changes in the stomatal limitation of photosynthesis: empirical**
2 **support for an optimality principle**

3 **Aliénor Lavergne^{1,2,*}, Steve Voelker³, Adam Csank⁴, Heather Graven^{2,5}, Hugo J. de**
4 **Boer⁶, Valérie Daux⁷, Iain Robertson⁸, Isabel Dorado-Liñán⁹, Elisabet Martínez-**
5 **Sancho¹⁰, Giovanna Battipaglia¹¹, Keith J. Bloomfield¹, Christopher J. Still¹², Frederick**
6 **C. Meinzer¹³, Todd E. Dawson¹⁴, J. Julio Camarero¹⁵, Rory Clisby⁸, Yunting Fang¹⁶,**
7 **Annette Menzel¹⁷, Rachel M. Keen¹⁸, John S. Roden¹⁹, and I. Colin Prentice^{1,5,20,21}**

8
9 ¹Department of Life Sciences, Imperial College London, Silwood Park Campus, Buckhurst
10 Road, SL5 7PY, Ascot, UK

11 ²Department of Physics, Imperial College London, Exhibition Road, SW7 2AZ, London, UK

12 ³Department of Environmental and Forest Biology, SUNY College of Environmental Science
13 and Forestry, Syracuse, NY, USA

14 ⁴Department of Geography, University of Nevada-Reno, 1664 N. Virginia St., Reno, NV, USA

15 ⁵Grantham Institute – Climate Change and the Environment, Imperial College London,
16 Exhibition Road, SW7 2AZ, London, UK

17 ⁶Department of Environmental Sciences, Utrecht University, Utrecht, The Netherlands

18 ⁷Laboratoire des Sciences du Climat et de l'Environnement, CEA-CNRS-UVSQ, 91191 Gif-
19 sur-Yvette, France

20 ⁸Department of Geography, Swansea University, Swansea, SA2 8PP, UK

21 ⁹Forest Genetics and Ecophysiology Research Group, Technical University of Madrid, Madrid,
22 Spain

23 ¹⁰Swiss Federal Institute for Forest, Snow and Landscape Research WSL, Zürcherstrasse 111,
24 Birmensdorf 8903, Switzerland

25 ¹¹Department of Environmental, Biological and Pharmaceutical Sciences and Technologies,
26 University of Campania "L. Vanvitelli", Via Vivaldi, 81100, Caserta, Italy

27 ¹²Department of Forest Ecosystems & Society, Oregon State University, Corvallis, OR, USA

28 ¹³USDA Forest Service, Pacific Northwest Research Station, Corvallis, Oregon, USA

29 ¹⁴Department of Integrative Biology, University of California – Berkeley, Berkeley, CA, USA

30 ¹⁵Instituto Pirenaico de Ecología (IPE-CSIC), E-50192 Zaragoza, Spain

31 ¹⁶Institute of Applied Ecology, Chinese Academy of Sciences, Shenyang, 110016, China

32 ¹⁷Ecoclimatology, Department of Ecology and Ecosystem Management, Technische
33 Universitat Munchen, Freising, Germany

34 ¹⁸Division of Biology, Kansas State University, Manhattan, KS, USA

35 ¹⁹Department of Biology, Southern Oregon University, Ashland, OR, USA

36 ²⁰Department of Biological Sciences, Macquarie University, North Ryde, NSW 2109,
37 Australia

38 ²¹Department of Earth System Science, Tsinghua University, Beijing, 100084, China

39 *corresponding author: a.lavergne@imperial.ac.uk

40

41 Journal of submission: *New Phytologist*

42 Type: Regular research paper

43 Total word count (should be < 6,500): 6,444

44 Word counts for each section: Introduction: 1,505, Material and Methods: 2,212, Results:

45 810, Discussion: 1,917

46 Figures: 6

47 Table: 1

48 Supporting Information (SI): 3 Figures, 2 Tables and 5 Texts

49

50 **Summary:** 195 words

51 • The ratio of leaf-internal (c_i) to ambient (c_a) partial pressure of CO₂, defined here as χ ,
52 is an index of adjustments in both leaf stomatal conductance and photosynthetic rate to
53 environmental conditions. Measurements and proxies of this ratio can be used to
54 constrain vegetation models uncertainties for predicting terrestrial carbon uptake and
55 water use.

56 • We test a theory based on the least-cost optimality hypothesis for modelling historical
57 changes in χ over the 1951-2014 period, across different tree species and environmental
58 conditions, as reconstructed from stable carbon isotopic measurements across a global
59 network of 103 absolutely-dated tree-ring chronologies. The theory predicts optimal χ
60 as a function of air temperature, vapour pressure deficit, c_a and atmospheric pressure.

- 61 • The theoretical model predicts 39% of the variance in χ values across sites and years,
62 but underestimates the inter-site variability in the reconstructed χ trends, resulting in
63 only 8% of the variance in χ trends across years explained by the model.
- 64 • Overall, our results support theoretical predictions that variations in χ are tightly
65 regulated by the four environmental drivers. They also suggest that explicitly
66 accounting for the effects of plant-available soil water and other site-specific
67 characteristics might improve the predictions.

68

69

70 **Keywords:** leaf-internal CO₂ concentration, stable carbon isotopes, tree rings, optimality,
71 least-cost hypothesis, water use efficiency

72 1. Introduction

73 The net uptake of atmospheric CO₂ by the terrestrial biosphere, which acts as a sink for about
74 30% of anthropogenic CO₂ emissions, has helped to reduce the increase in atmospheric CO₂
75 concentration – and therefore has dampened climate change – since the beginning of the
76 industrial era (Le Quéré *et al.*, 2018). However, it is still unclear how atmospheric CO₂, climate,
77 and other environmental changes will influence the future strength of the terrestrial carbon sink
78 (Ciais *et al.*, 2013; Ballantyne *et al.*, 2015; Schimel *et al.*, 2015). It has been suggested that the
79 magnitude of net terrestrial carbon uptake is likely to decline in the future as a result of various
80 mechanisms including resource limitations on the CO₂ ‘fertilization’ effect due to nitrogen
81 availability (Reich *et al.*, 2006; Reich & Hobbie, 2013), reduced water availability due to
82 changes in the hydrological cycle (Zhao & Running, 2010; Humphrey *et al.*, 2018; Green *et al.*,
83 2019), or enhanced turnover of soil carbon due to warming (Knorr *et al.*, 2005; Li *et al.*,
84 2018). Yet, the extent to which these processes might affect the terrestrial carbon sink is still
85 largely unknown, especially when considering the real possibility of plant adaptation and
86 acclimation that may occur over decadal to longer timescales. Current models of the terrestrial
87 biosphere incorporate different formulations of the underlying processes, including
88 photosynthesis and leaf gas exchanges responses to varying CO₂ concentrations (Rogers *et al.*,
89 2017), the impact of soil moisture stress on photosynthesis and stomatal conductance (De
90 Kauwe *et al.*, 2013), and carbon allocation and turnover (De Kauwe *et al.*, 2014) – leading to
91 large differences in simulated terrestrial CO₂ uptake and future climate change. New metrics
92 and proxies of key biological processes are thus needed to improve and reduce uncertainties in
93 terrestrial models.

94 The ratio (hereafter termed χ) of leaf-internal (c_i) to ambient (c_a) partial pressure of CO₂ is a
95 key metric of physiological function in plant leaves being determined by both stomatal
96 conductance on the short term and photosynthetic biochemical capacity on longer time scales
97 (Farquhar *et al.*, 1982). Thus, χ is the key variable for the study of carbon uptake. Under some
98 conditions it can also provide insights into changes in intrinsic water-use efficiency (iWUE),
99 i.e. the ratio of photosynthesis to stomatal conductance, defined as $iWUE = c_a (1-\chi)/1.6$
100 (Ehleringer *et al.*, 1993). As there are many other definitions of water use efficiency by plants,
101 each with different meanings (Lavergne *et al.*, 2019), analysis of data directly in terms of χ is
102 preferred here. Plants assimilate the heavier ¹³CO₂ molecules less readily than ¹²CO₂ because
103 of their slower diffusion through the stomata and preferential fixation of ¹²CO₂ by Rubisco,

104 resulting in a discrimination against ^{13}C compared to ^{12}C , defined as $\Delta^{13}\text{C}$ (Park & Epstein,
105 1960). In C_3 plants, $\Delta^{13}\text{C}$ is principally determined by χ . Thus, reconstructing long-term
106 effective values of χ from $\Delta^{13}\text{C}$ derived from stable isotope $^{13}\text{C}/^{12}\text{C}$ ratio ($\delta^{13}\text{C}$) measured in
107 plant materials (including tree rings), or even in atmospheric CO_2 , can offer valuable insights
108 into stomatal and photosynthetic adjustments to environmental conditions. As air masses are
109 transported and mixed rapidly in the turbulent lower atmosphere, $\Delta^{13}\text{C}$ values inferred from
110 atmospheric $\delta^{13}\text{CO}_2$ are representative of processes occurring at regional (Ballantyne *et al.*,
111 2010; Peters *et al.*, 2018) or global (Keeling *et al.*, 2017) scales, while values derived from tree
112 rings reflect ecophysiological processes at the individual plant level. Thus, $\delta^{13}\text{C}$ data from
113 different sources can in principle be used to evaluate and improve the representation of stomatal
114 and photosynthetic behaviour in models at different spatial scales. However, atmospheric
115 $\delta^{13}\text{CO}_2$ is also influenced by many other processes, such as ocean-atmosphere gas exchange
116 and isotope disequilibrium fluxes (Keeling *et al.*, 2017), complicating the derivation of long-
117 term changes in χ using atmospheric data.

118 Formulations for $\Delta^{13}\text{C}$ have been included in vegetation models (Saurer *et al.*, 2014; Frank *et*
119 *al.*, 2015; Raczka *et al.*, 2016; Keller *et al.*, 2017) and evaluated using existing observations as
120 recommended by the Coupled Model Intercomparison Project Phase 6 (CMIP6), which
121 coordinates current Earth System modelling activities internationally (Eyring *et al.*, 2016;
122 Jones *et al.*, 2016). Yet some recent studies have shown that current models overestimate the
123 decrease in $\Delta^{13}\text{C}$ (and the associated increase in water-use efficiency) over the 20th century
124 (Keller *et al.*, 2017) or simulate an increase in both $\Delta^{13}\text{C}$ and water-use efficiency at leaf level,
125 which is inconsistent with biological theory (Raczka *et al.*, 2016). These studies demonstrate
126 that $\Delta^{13}\text{C}$ can reveal explicit biases within the models. Errors in the simulation of $\Delta^{13}\text{C}$ can,
127 however, be difficult to attribute to particular processes. Incomplete, empirical descriptions of
128 the processes determining χ in vegetation models and incorrect assumptions about key
129 parameters in the model of photosynthesis may cause discrepancies between observed and
130 predicted $\Delta^{13}\text{C}$. Many models assign fixed parameter values to different plant functional types
131 (PFTs) (Rogers *et al.*, 2017), but this approach overlooks the ability of plants (within any one
132 PFT) to acclimate or adapt to environmental changes (Wullschleger *et al.*, 2014; Martínez-
133 Sancho *et al.*, 2018; Dorado-Liñán *et al.*, 2019). Also, some of the processes linking c_i to $\Delta^{13}\text{C}$
134 have been neglected. The potential impact of fractionations during the transport of CO_2 from
135 the intercellular space to the chloroplasts, and during photorespiration have been described

136 (Ubierna & Farquhar, 2014), and may be important to include when analysing historical trends
137 (Seibt *et al.*, 2008; Keeling *et al.*, 2017; Schubert & Jahren, 2018; Lavergne *et al.*, 2019).
138 Accordingly, there is a need to probe the assumptions about leaf gas exchange incorporated in
139 such models, to include the known physiological and environmental processes influencing
140 $\Delta^{13}\text{C}$, and to evaluate the resulting simulations with long-term carbon isotope data.

141 Simpler analytical models can provide an integrative approach to understand whole-plant
142 responses to environmental changes via the general hypothesis that plants optimize their
143 physiology towards maximizing fitness (Medlyn *et al.*, 2013; Dewar *et al.*, 2018). However,
144 the trade-off between the benefits and costs of stomatal opening (carbon gain at the expense of
145 water loss) and investments in photosynthetic biochemistry (requiring nitrogen and energy) is
146 still not completely understood; in particular, the specific nature of the costs remains an open
147 question. Different optimization hypotheses for the control of stomatal conductance have been
148 proposed – reviewed in Buckley (2017) and Dewar *et al.* (2018) – that make different
149 predictions of stomatal responses to the environment. The Cowan-Farquhar optimality
150 hypothesis states that leaves maximize the difference between photosynthesis and the carbon
151 cost of transpiration, i.e. $A - E/\lambda$, where A is the photosynthesis rate, E is the rate of
152 transpiration and λ is an ‘exchange rate’ between carbon and water (Cowan & Farquhar, 1977;
153 Katul *et al.*, 2010; Buckley & Schymanski, 2014; Sperry *et al.*, 2017). λ has usually been
154 determined as a function of soil moisture (Manzoni *et al.*, 2013) and of xylem water potential
155 (Wolf *et al.*, 2016; Sperry *et al.*, 2017). The Cowan-Farquhar optimality hypothesis, however,
156 does not account for the costs of maintaining both water flow and photosynthetic capacity
157 (Givnish, 1986). Following the least-cost optimality hypothesis proposed by Wright *et al.*
158 (2003), Prentice *et al.* (2014) introduced the alternative criterion that leaves minimize the
159 summed unit costs of transpiration and carboxylation, i.e. $(a_E E + b_V V_{\text{cmax}})/A$, where a_E is the
160 sapwood maintenance cost per unit of transpiration capacity and b_V is the cost associated with
161 the maintenance of photosynthetic (carboxylation) capacity (V_{cmax}) (Rogers, 2014). Dewar *et al.*
162 (2018) analysed another criterion, following Givnish (1986), whereby the cost of stomatal
163 opening arises from nonstomatal reductions in photosynthesis induced by leaf water stress. The
164 authors explored different hypotheses in which reduced leaf water potential leads to a reduction
165 either in V_{cmax} or in mesophyll conductance. Predicted stomatal responses were broadly similar
166 to those derived from the least-cost optimality hypothesis (Dewar *et al.*, 2018), although the
167 reduction of V_{cmax} rather than mesophyll conductance provided a better fit across different PFTs
168 (Gimeno *et al.*, 2019).

169 Here we test the theoretical framework implied by the least-cost optimality hypothesis for
170 predicting long-term changes in χ across the globe, during a period of steadily increasing c_a
171 (around 85 ppm over 1951–2014). Spatial patterns of χ predicted by the least-cost hypothesis
172 have been supported by analyses of leaf $\delta^{13}\text{C}$ data at the regional (Bloomfield *et al.*, 2019) and
173 global (Wang *et al.*, 2017b) scales. However, simulations of χ and its trends over the past
174 decades using this model still await evaluation against long-term observations. Here we first
175 reconstruct changes in χ over 1951–2014 using a global tree-ring $\delta^{13}\text{C}$ ($\delta^{13}\text{C}_{\text{TR}}$) network of 103
176 sites. We then compare model predictions and reconstructions for their spatial and temporal
177 patterns and examine the sensitivity of predicted and isotope-derived χ to the environmental
178 drivers of the model and other constraints. Our aim is to address the following questions: (1)
179 Can temporal variations in χ – as indexed by long-term $\delta^{13}\text{C}_{\text{TR}}$ measurements – be predicted
180 by the least-cost hypothesis? (2) How well do these predictions of χ reproduce the ratio’s
181 observed dependency on environmental drivers? Finally, (3) are there any other potential
182 environmental controls on χ that should be considered in order to improve these predictions?
183

184 2. Material and methods

185 a. Observational dataset of χ

186 We compiled 103 absolutely-dated $\delta^{13}\text{C}_{\text{TR}}$ chronologies from published and unpublished
187 materials representing different PFTs (DBF: deciduous broadleaf forest ($n = 29$) and ENF:
188 evergreen needleleaf forest ($n = 74$)) and environmental contexts in the temperate and boreal
189 zones, with at least 30 years of records over the 1951–2014 period when most data were
190 available (Fig. 1; Table S1). $\delta^{13}\text{C}_{\text{TR}}$, i.e. the ratio of ^{13}C to ^{12}C of the wood component compared
191 to an internationally accepted standard material, was derived from cellulose (with just two
192 exceptions where bulk wood was used) and from either the whole ring (WR, $n = 65$; including
193 both earlywood and latewood) or only latewood (LW, $n = 38$; Table S1). The analytical error
194 in the $\delta^{13}\text{C}_{\text{TR}}$ measurements was typically $\pm 0.15\text{‰}$. $\Delta^{13}\text{C}$ for each series was calculated as:

$$195 \quad \Delta^{13}\text{C} = \frac{\delta^{13}\text{C}_{\text{CO}_2} - (\delta^{13}\text{C}_{\text{TR}} - d)}{1 + (\delta^{13}\text{C}_{\text{TR}} - d)/1000} \quad \text{Eqn 1}$$

196 where $\delta^{13}\text{C}_{\text{CO}_2}$ is the stable isotopic composition of atmospheric CO_2 in the year of ring
197 formation, and d (‰) quantifies the sum of discriminations beyond those associated with the
198 production of the primary photosynthetic assimilates: 1.9‰ between leaf organic matter and

199 bulk wood (Badeck *et al.*, 2005), and $2.1 \pm 1.2\text{‰}$ between leaf organic matter and α -cellulose
 200 (Frank *et al.*, 2015). For each year, $\Delta^{13}\text{C}$ was used to derive χ_{iso} (i.e. the isotope-derived χ) with
 201 the model from Farquhar *et al.* (1982) including an explicit fractionation term for
 202 photorespiration as recommended by several studies (e.g. Ubierna & Farquhar, 2014; Schubert
 203 & Jahren, 2018; Lavergne *et al.*, 2019) but assuming effectively infinite boundary layer and
 204 mesophyll conductances, and negligible fractionation during mitochondrial respiration
 205 (Ghashghaie *et al.*, 2003; Evans & Von Caemmerer, 2013):

$$206 \quad \Delta^{13}\text{C} = a + (b - a)\chi_{\text{iso}} - f \frac{\Gamma^*}{c_a} \quad \text{Eqn 2}$$

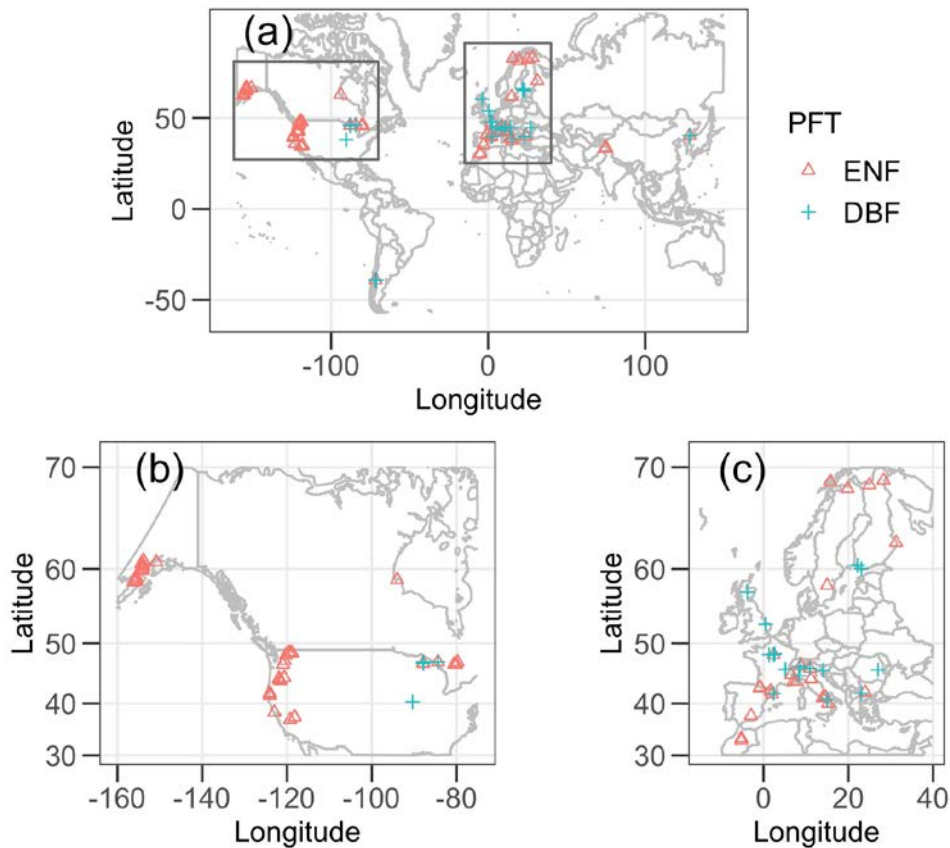
207 where a , b and f represent in turn: isotope fractionations due to CO_2 diffusion in air (4.4‰:
 208 Craig, 1953), effective Rubisco carboxylation (26-30‰) and photorespiration (8-16‰;
 209 Ubierna & Farquhar, 2014), respectively. Γ^* (Pa) is the CO_2 compensation point in the absence
 210 of mitochondrial respiration, i.e. the value of c_i at which the rate of photosynthetic CO_2 uptake
 211 equals that of photorespiratory CO_2 evolution, calculated from the temperature and pressure
 212 response: $\Gamma^* = \Gamma^*_{25} P_{\text{atm}}/P_0 \exp[\Delta H_a.(T - 298)/(R.T.298)]$, with Γ^*_{25} the photorespiratory
 213 compensation point at 25°C, ΔH_a the activation energy for Γ^* (Bernacchi *et al.*, 2001), T the
 214 temperature, R the universal gas constant (Moldover *et al.*, 1988), and P_{atm} and P_0 the ambient
 215 and sea-level atmospheric pressures. Note that we did not consider mesophyll conductance (g_m)
 216 in our calculations because information on g_m , which is highly variable between species (von
 217 Caemmerer & Evans, 2015) and may fluctuate over long time periods (Flexas *et al.*, 2008), is
 218 generally lacking. Nevertheless, given the influence of g_m in the full discrimination model, we
 219 provide a sensitivity analysis in the Supporting Information (Text S1 and Fig. S1).

220 From Eqns 1 and 2, χ_{iso} can be written as:

$$221 \quad \chi_{\text{iso}} = \frac{\left(\frac{\delta^{13}\text{CO}_2 - (\delta^{13}\text{C}_{\text{TR}} - d)}{1 + (\delta^{13}\text{C}_{\text{TR}} - d)/1000}\right) - a + f \frac{\Gamma^*}{c_a}}{b - a} \quad \text{Eqn 3}$$

222 The choice of the values in Eqn 3 for the fractionation factors related to Rubisco carboxylation
 223 (b), photorespiration (f) and post-photosynthetic processes (d) does not affect the trend
 224 estimates of χ_{iso} but only modulates the mean χ_{iso} levels (Fig. S1). In the following, we have
 225 used the mean values from their range of uncertainties of $b = 28\text{‰}$ and $f = 12\text{‰}$ (Ubierna &
 226 Farquhar, 2014). Post-photosynthetic fractionations were assumed equal for all species ($d =$
 227 2.1‰ for cellulose and 1.9‰ for bulk wood) because information quantifying these effects for

228 individual species is sparse (Seibt *et al.*, 2008; Wingate *et al.*, 2008; Bowling *et al.*, 2008;
 229 Gessler *et al.*, 2014). Thus, we inevitably made some approximations that may have
 230 contributed to uncertainty in the reconstructed χ_{iso} values. Finally, to minimize the potential
 231 effect of mixing and turnover of non-structural carbohydrate pools of different ages and
 232 metabolic history in $\delta^{13}\text{C}_{\text{TR}}$ (Gessler *et al.*, 2014), we have aggregated the resulting χ_{iso} series
 233 into boxcar averages over a five-year period.
 234



235
 236 **Fig. 1** (a) Location of the selected 103 tree-ring sites with carbon isotopic measurements (see
 237 Table S1 for details). Zoom over North America (b) and Europe (c) where the network is
 238 denser. PFT: plant functional type (DBF: deciduous broadleaf forest ($n = 29$) and ENF:
 239 evergreen needleleaf forest ($n = 74$)).

240

241

242 **b. Prediction of χ following the optimality hypothesis**

243 i. The theoretical model

244 The theory to predict χ (χ_{pred} , hereafter) following the least-cost optimality hypothesis has been
 245 introduced (Prentice *et al.*, 2014; Wang *et al.*, 2017b; Stocker *et al.*, 2019a) and applied in

246 several recent studies (Dong *et al.*, 2017; Wang *et al.*, 2017a; Togashi *et al.*, 2018; Bloomfield
 247 *et al.*, 2019; Smith *et al.*, 2019). One of the strengths of the model is that there is no distinction
 248 among PFTs and biomes, except for the well-established differences between C₃ and C₄ plants,
 249 and therefore no fixed parameter defines the behaviour of the vegetation as in most current
 250 models (Rogers *et al.*, 2017). Thus, vegetation functions are allowed to evolve freely with
 251 environmental changes. The model is driven by P_{atm} , observed air temperature (T), vapour
 252 pressure deficit (D) and c_a at the selected time step (here, monthly) as follows:

$$253 \quad \chi_{\text{pred}} = \frac{c_i}{c_a} = \frac{\Gamma^*}{c_a} + \left(1 - \frac{\Gamma^*}{c_a}\right) \frac{\xi}{\xi + \sqrt{D}} \quad \text{Eqn 4a}$$

254 where

$$255 \quad \xi = \sqrt{\beta \frac{K + \Gamma^*}{1.6\eta^*}} \quad \text{Eqn 4b}$$

256 ξ modulates the sensitivity of χ_{pred} to D , β (unitless) is the ratio of cost factors for carboxylation
 257 and transpiration (b_V/a_E) at 25°C, η^* is the viscosity of water relative to its value at 25°C, and
 258 K (Pa) is the effective Michaelis constant for Rubisco-limited photosynthesis at ambient partial
 259 pressure of O₂ (O , Pa) given by:

$$260 \quad K = K_C \left(1 + \frac{O}{K_O}\right) \quad \text{Eqn 5}$$

261 where K_C (Pa) and K_O (Pa) are the Michaelis constants of Rubisco for carboxylation and
 262 oxygenation, respectively. K and η^* are known functions of T and P_{atm} , and can be estimated
 263 following Bernacchi *et al.* (2001) and Huber *et al.* (2009), respectively. P_{atm} is calculated from
 264 elevation (z) following Allen *et al.* (1998). Only one free parameter is used here, i.e. β , whose
 265 values were estimated independently for ENF and DBF based on the tree-ring network of $\delta^{13}\text{C}$
 266 data using Eqn 4 under the mean environmental conditions over the studied period (see Text
 267 S2; $\beta_{\text{ENF}} = 176$ and $\beta_{\text{DBF}} = 191$). Note that our assumption of a constant β is a practical
 268 approximation based on environmental conditions as β may vary over time, e.g., due to changes
 269 in soil moisture content (Stocker *et al.*, 2018, 2019b). Thus, the theoretical model does not
 270 explicitly account for potential effects of changes in soil moisture on χ (the potential impacts
 271 of soil moisture limitation on χ are discussed further below). Also, as $c_a > \Gamma^*$ under field
 272 conditions, the theory predicts that χ is only slightly dependent on c_a . Overall, optimal χ

273 following the theory is expected to increase with increasing T but to decrease with increasing
274 D and c_a , and decreasing P_{atm} (i.e. increasing z) (Wang *et al.*, 2017a).

275

276 ii. Driving data

277 Latitude and longitude were used to extract minimum and maximum temperatures (T_{min} and
278 T_{max} , °C) and actual vapour pressure (e_a , hPa) for each site from monthly 0.5° resolution data
279 provided by the Climatic Research Unit (CRU TS4.01; Harris *et al.*, 2014). When not provided
280 by the authors (Table S1), z (km) used to infer P_{atm} were obtained from the WATCH Forcing
281 Data methodology applied to ERA-Interim data (WFDEI) with 0.5° resolution (Weedon *et al.*,
282 2014) using the latitude and longitude of the site. Estimated z values from WFDEI dataset were
283 in reasonably good agreement with those provided by authors, when available ($r^2 = 0.77$, $p <$
284 0.001 ; Fig. S2). Monthly atmospheric CO₂ concentrations (in ppm) for the 1958-2014 period
285 were derived from in-situ direct measurements provided by the Scripps Institution of
286 Oceanography (http://scrippsco2.ucsd.edu/data/atmospheric_co2/). For the 1951-1958 period,
287 we interpolated the monthly CO₂ values using the mean seasonal cycle recorded over 1958-
288 2014 and the yearly CO₂ values from a merged product based on ice core data and in-situ direct
289 measurements (Fig. S3). The c_a dataset was first corrected for the elevation effect and converted
290 into Pascals prior to being used for the analyses, as: c_a (Pa) = 10^{-6} [CO₂]_{ppm} P_{atm} . Atmospheric
291 $\delta^{13}\text{CO}_2$ data for the historical period of interest were extracted from a recent compilation by
292 Graven *et al.* (2017).

293 We calculated the monthly mean daytime air T (T_{daytime} , °C) to consider only the part of the day
294 when photosynthesis occurs, as:

$$295 \quad T_{\text{daytime}} = T_{\text{max}} \left\{ \frac{1}{2} + \frac{[\sqrt{(1-x^2)}]}{2\arccos x} \right\} + T_{\text{min}} \left\{ \frac{1}{2} - \frac{[\sqrt{(1-x^2)}]}{2\arccos x} \right\} \quad \text{Eqn 6a}$$

296 where

$$297 \quad x = -\tan \phi \tan \delta \quad \text{Eqn 6b}$$

298 with ϕ the latitude (°) and δ the average solar declination for the month (Jones, 2013).

299 Given our hypothesis of infinite boundary layer conductance in Eqn 3, we assumed equality of
300 leaf and air temperatures. Monthly mean daytime D (D_{daytime} , kPa) was calculated following
301 Allen *et al.* (1998) using T_{daytime} , monthly mean e_a and P_{atm} as:

$$D_{\text{daytime}} = 0.611e^{\left[\frac{8.635 \cdot T_{\text{daytime}}}{237.3 + T_{\text{daytime}}}\right]} - 0.10e_a \frac{P_{\text{atm}}}{P_0} \quad \text{Eqn 7}$$

303

304 **c. Model evaluation**

305 For evaluating model predictions against reconstructions, the monthly χ_{pred} values initially
 306 calculated following Eqn 4 using the monthly mean daytime values of climate predictors (i.e.
 307 T_{daytime} , D_{daytime}) and c_a were aggregated as medians over the most productive months of the
 308 growing season to produce the growing-season χ_{pred} series. At each site the peak growing-
 309 season months, when most of the carbon to build the tree ring is fixed, were estimated based
 310 on a literature review (see Table S1). When no information was available, we assumed a
 311 growing season centred over summer months, i.e. June-August for the Northern hemisphere.
 312 We then aggregated the resulting yearly χ_{pred} series as five-year boxcar averages before
 313 comparing them with independently estimated, also five-year averaged χ_{iso} .

314 All statistical analyses were conducted in the open-source statistical environment R (R Core
 315 Team & R Development Core Team, 2018). We first compared the spatial and temporal
 316 patterns of χ between reconstructions and predictions before investigating potential biases in
 317 the predictions. The agreement between χ_{pred} and χ_{iso} values was assessed using the adjusted
 318 R -squared (R^2_{adj}), the root mean square error (RMSE), the Akaike information criterion (AIC;
 319 Akaike, 1973) and the Bayesian information criterion (BIC) using the R package **performance**
 320 (Lüdecke *et al.*, 2019); overall, lower RMSE, AIC and BIC values indicating greater
 321 explanatory power. The temporal changes in χ at each site for both reconstructions and
 322 predictions were quantified using the Theil-Sen estimator from the R package **trend** (Pohlert,
 323 2018), which calculates a trend as the median of the slopes of all lines through pairs of points
 324 (Sen, 1968). Before estimating Theil-Sen trends, χ_{pred} and χ_{iso} values were converted into
 325 percentages of changes in χ relative to the site mean, in order to make the trends more
 326 comparable with each other:

$$\chi (\%) = \frac{\chi_t - \chi_{\text{mean}}}{\chi_{\text{mean}}} \times 100 \quad \text{Eqn 8}$$

328 where χ_t and χ_{mean} are the values for χ at the time resolution considered (five years) and for the
 329 whole 1951-2014 period, respectively. The resulting χ trend estimates were compared between
 330 reconstructions and predictions using different linear regression models. We first applied the

331 ordinary least squares (OLS) method for reducing the residuals in the linear regression and then
 332 applied the M-estimators method to perform robust linear regressions (RLM) using the R
 333 package MASS (Venables & Ripley, 2002). The M-estimators method is generally less
 334 sensitive to outliers than the OLS method. To assess the effect of temporal changes in growing-
 335 season mean T_{daytime} and D_{daytime} (hereafter T_g and D_g , respectively) on χ trends, we additionally
 336 calculated T_g and D_g trends following the same approach as described above.

337 As a further examination of the skill of the least-cost hypothesis, we investigated the relative
 338 dependencies of χ_{pred} and χ_{iso} values on the four drivers of the model using multiple linear
 339 regression. To do so, we first calculated the logit-transformed χ_{iso} and χ_{pred} values as: $\text{logit } \chi =$
 340 $\ln [\chi / (1 - \chi)]$. Logit transformation stabilizes variance in quantities with a (0,1) range and also
 341 simplifies the comparison of the sensitivity of χ to environmental variables. We also estimated
 342 the model bias (B) in χ predictions at each site as:

$$343 \quad B = \frac{\chi_{\text{pred}} - \chi_{\text{iso}}}{\chi_{\text{iso}}} \times 100 \quad \text{Eqn 9}$$

344 Linear regressions of logit χ_{iso} , logit χ_{pred} and B against the four primary drivers (T_g , natural
 345 log-transformed D_g , c_a and z) as predictors were applied using OLS. The variance explained by
 346 each of the fixed effects was calculated via commonality analyses using the R package yhat
 347 (Nimon *et al.*, 2013). We also tested two linear mixed-effect models (Bolker *et al.*, 2009; Zuur
 348 *et al.*, 2009) using the R package lme4 (Bates *et al.*, 2015) that included the four above-
 349 mentioned fixed-effects but also a random effect related to site to account for site grouping on
 350 variance partitioning. One model included only random intercepts, while another included both
 351 random intercepts and slopes. The variance explained by the fixed effects and that explained
 352 by the entire models, including both fixed and random effects, were also calculated.

353 Finally, to investigate the potential influences of soil water availability on χ , we tested different
 354 multiple linear models of logit χ_{iso} and B that included the primary drivers of the least-cost
 355 hypothesis and one index of plant-available soil water as predictors. Three alternative indices
 356 of drought severity or soil water availability were tried: 1) a drought index based on climate
 357 water balance (the Standardized Precipitation-Evapotranspiration Index, SPEI) inferred from
 358 the 0.5° gridded monthly SPEIbase dataset (Beguería *et al.*, 2010); 2) the surface soil moisture
 359 content (θ , $\text{m}^3 \text{m}^{-3}$) data extracted at each site from the 0.25° resolution product of the European
 360 Space Agency Climate Change Initiative (Dorigo *et al.*, 2017); and 3) an estimate of the ratio
 361 of actual evapotranspiration to equilibrium evapotranspiration (Priestley-Taylor coefficient, α)

362 calculated at each site using the SPLASH model (Davis *et al.*, 2017) (see Text S3 for more
363 details).

364 All linear models were compared using analysis of variance (ANOVA), RMSE, AIC and BIC.
365 The partial residuals of most models were computed using the R package *effects* (Fox *et al.*,
366 2018) and the respective residual plots were visually examined against environmental
367 variables.

368

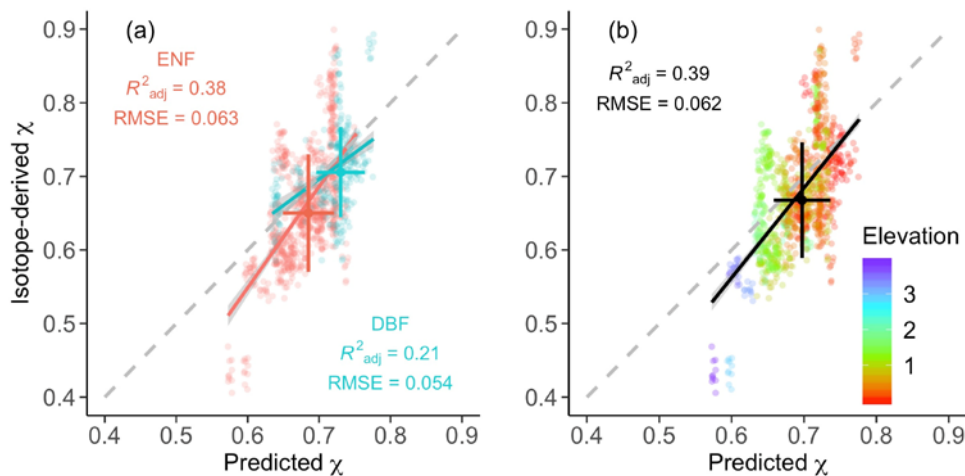
369 3. Results

370

371 Model-data comparison of χ values

372 Over the studied 1951–2014 period, χ_{pred} and χ_{iso} values were in reasonable agreement ($R^2_{\text{adj}} =$
373 0.39, RMSE = 0.062, AIC = -3000, BIC = -3000, $p < 0.001$; Fig. 2b), but were more consistent
374 for ENF than DBF sites ($R^2_{\text{adj}} = 0.38$, RMSE = 0.063, AIC = -2140, BIC = -2126 for ENF
375 versus $R^2_{\text{adj}} = 0.21$, RMSE = 0.054, AIC = -907, BIC = -896 for DBF, $p < 0.001$; Fig. 2a). χ_{pred}
376 values from high-elevation sites (i.e. with low P_{atm}) tended to be lower than those from low-
377 elevation sites (i.e. high P_{atm}), although the reconstructed values did not show this distinction
378 as clearly as the predicted values (Fig. 2b).

379



380

381 **Fig. 2** Predicted versus isotope-derived five-year boxcar averages of χ over 1951-2014. Median
382 and standard deviations are shown for each PFT (a) or for all PFTs (b). The bold lines are the
383 ordinary least-squares (OLS) regressions for each PFT (a) or combined (b). The dashed grey
384 line is the 1:1 line. DBF: deciduous broadleaf forests ($n = 29$), ENF: evergreen needleleaf

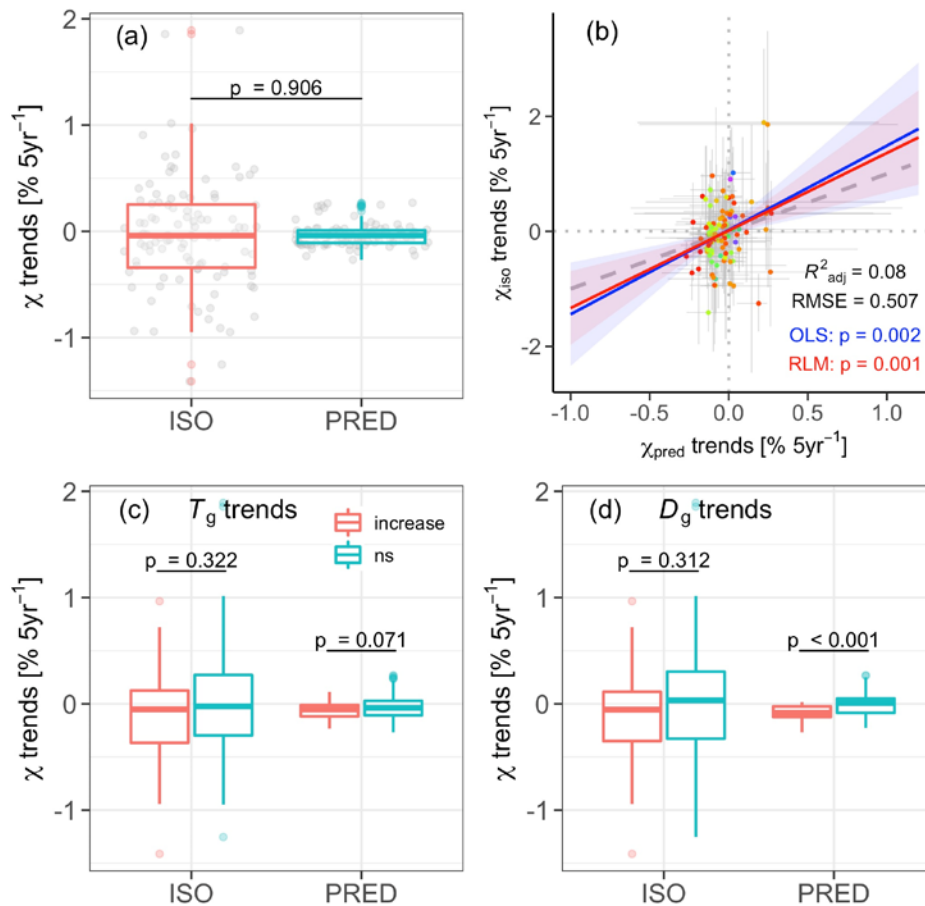
385 forests ($n = 74$). R^2_{adj} , adjusted r-squared ($p < 0.001$); RMSE, root mean square error of the
386 predictions. Elevation is in km.

387

388 **Model-data comparison of long-term trends in χ**

389 The median χ trends across sites were not significantly different from zero, either for the
390 isotope-based reconstructions (ranging across sites between -1.41 and 1.89% 5yr⁻¹) or for the
391 model predictions (ranging across sites between -0.27 and 0.27% 5yr⁻¹) ($p > 0.20$; Student's t
392 test; Fig. 3a). These results indicate that on average across sites, both χ_{iso} and χ_{pred} stayed nearly
393 constant while c_a increased by 2.05% 5yr⁻¹. Reconstructed and predicted χ trends were not
394 significantly different ($p = 0.906$; Student's t test). However, the variability of χ trends between
395 sites was larger in χ_{iso} than in χ_{pred} (interquartile range IQR = 0.60 versus 0.12; $p < 0.001$; F
396 test). No significant differences in χ_{iso} trends were detected between ENF and DBF series or
397 between latewood and whole ring series ($p > 0.40$; Student's t test). χ trends tended to be lower
398 at sites with increase in T_g and D_g , but these differences were only significant for the predicted
399 trends (Fig. 3c-d). Predicted and isotope-derived historical χ trends were only slightly related
400 to each other for all sites ($R^2_{\text{adj}} = 0.08$, RMSE = 0.507, AIC = 159, BIC = 166), as shown using
401 either OLS or RLM ($p < 0.003$; Fig. 3b). The relationship between χ_{iso} and χ_{pred} trends was
402 mainly driven by ENF sites ($R^2_{\text{adj}} = 0.11$, RMSE = 0.135, AIC = -78, BIC = -73, $p = 0.003$ for
403 ENF versus $R^2_{\text{adj}} = 0.03$, RMSE = 0.069, AIC = -67, BIC = -63, $p = 0.199$ for DBF).

404



405

406 **Fig. 3** Temporal changes in isotope-derived (ISO) and predicted (PRED) χ over 1951-2014 for
 407 the selected 103 tree-ring sites (see Table S1). The Theil-Sen trends of the % of changes relative
 408 to the site mean (% 5yr⁻¹) are presented considering all sites (a-b), or at each site depending on
 409 the historical trends in T_g (c) or D_g (d) (ns: non-significant trend, increase: positive trend). In
 410 (a), (c) and (d), the p-values from the Student's t tests performed between the different groups
 411 of trends are indicated. In (b), the 95% confidence intervals of the Theil-Sen trends are shown
 412 in light grey. The dashed grey line is the 1:1 line. The coloured lines with associated 95%
 413 confidence intervals are for different regression models: ordinary least squares (OLS) and
 414 robust (RLM) linear models. The p-value for these models are indicated. R^2_{adj} , adjusted r-
 415 squared; RMSE, root mean square error of the predictions.

416

417

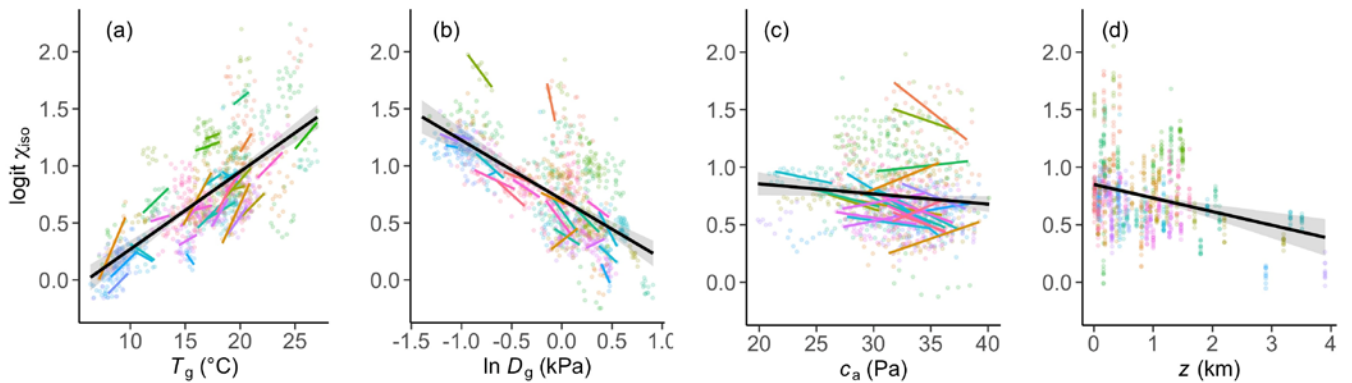
418 **Model-data comparisons against environmental drivers**

419 The partial residuals of logit χ_{iso} values increased with increasing T_g but decreased with
 420 increasing $\ln D_g$, c_a and z (i.e. decreasing P_{atm}) consistent with those of logit χ_{pred} (Table 1 and
 421 Fig. 4). When ignoring c_a as environmental driver of χ_{iso} , the variance explained by the

422 statistical model was similar to the one including c_a ($R^2_{\text{adj}} = 0.37$; see Table S2), the second
 423 model being only slightly improved (ANOVA test, $p = 0.036$). The relatively small
 424 contribution to the explained variance of the unique effect of c_a compared to the other drivers
 425 (Table 1) suggests that c_a had only a minor effect on χ_{iso} . When significant, the logit χ_{iso}
 426 responses to changing T_g , $\ln D_g$ and c_a varied and diverged from the general pattern at some
 427 sites (Figs 4a-c), however no clear pattern for these discrepancies emerged.

428 The linear mixed-effects models for logit χ_{iso} with T_g , $\ln D_g$, c_a and z (indexing P_{atm}) as fixed
 429 effects, and site as a random effect, performed better than the model considering only fixed
 430 effects (lower AIC and BIC, significant ANOVA test, $p < 0.001$; $R^2_{\text{cond}} = 0.94$ versus $R^2_{\text{adj}} =$
 431 0.39 ; Tables 1 and S2a). The model with random intercepts and slopes yielded lower AIC and
 432 BIC values than the one with only random intercepts. Both models, however, tended to assign
 433 most of the variance in logit χ_{iso} to the random effects (around 64%), whereas the fixed effects
 434 only contributed around 30% of the variance (Table S2a).

435



436

437 **Fig. 4** Partial residual plots showing temporal and spatial variations in the five-year boxcar
 438 average of logit χ derived from tree-ring stable carbon isotope data as a function of growing-
 439 season average climate variables (a, daytime temperature T_g ; b, natural log-transformed vapour
 440 pressure deficit D_g), c, partial pressure of CO_2 corrected for elevation effect (c_a) and d, elevation
 441 (z) indexing P_{atm} during 1951-2014. The colours correspond to sites. The solid colour lines
 442 indicate the modelled response from the multiple linear regression models for each site, while
 443 the solid black lines are those for all sites combined (see Table 1 for statistics). The grey shaded
 444 area represents the 95% confidence interval of the regression. Only significant trends at 95%
 445 ($p < 0.05$) are shown.

446

447

448 **Table 1.** Summary statistics for the environmental dependencies of reconstructed and predicted
 449 logit χ . ΔT_g is the difference between growing-season mean temperature T_g and 25°C. Standard
 450 error (SE), Student's t test (t-value), contributions to the explained variance (R^2) of unique
 451 effect (Unique) and both unique and common effects (Total) for each environmental driver (in
 452 % of R^2), adjusted r-squared (R^2_{adj}), root mean square error (RMSE), Akaike information
 453 criterion (AIC) and Bayesian information criterion (BIC). The statistical significance of the
 454 models is indicated ($p < 0.001$, *** and $p < 0.05$, *).

455

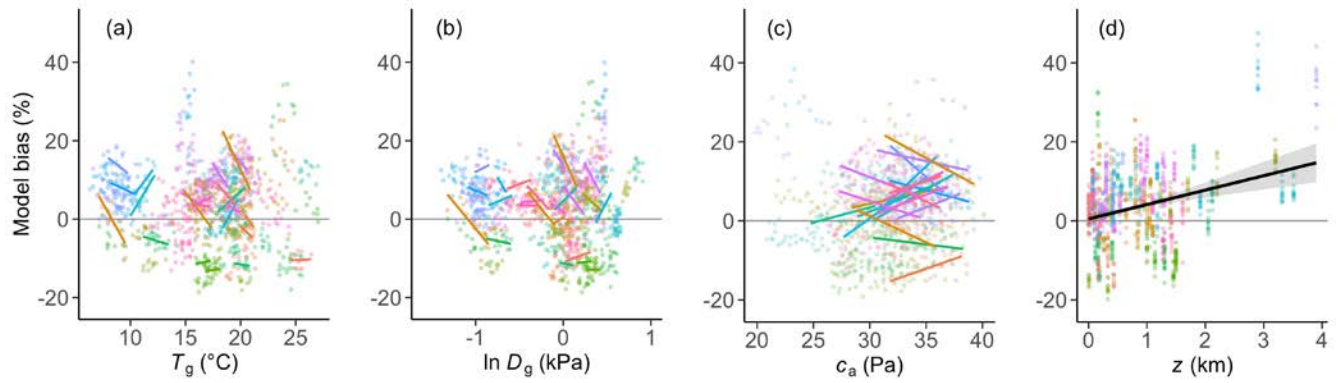
	Predictor	Estimate	SE	t-value	Unique	Total	R^2_{adj}	RMSE	AIC	BIC
Recons- truction	ΔT_g	0.068***	0.005	12.745	24.65	14.63	0.37***	0.306	522	552
	$\ln D_g$	-0.520***	0.056	-9.202	12.85	6.03				
	z	-0.118***	0.026	-4.458	3.02	67.93				
	c_a	-0.009*	0.004	-2.096	0.67	36.28				
	Intercept	1.625***	0.145	10.924						
Prediction	ΔT_g	0.061***	<0.001	153.40	33.04	13.15	0.98***	0.023	-5208	-5178
	$\ln D_g$	-0.504***	0.004	-119.95	20.20	7.08				
	z	-0.040***	0.002	-20.17	0.57	62.33				
	c_a	-0.004***	<0.001	-11.71	0.19	35.39				
	Intercept	1.401***	0.011	126.39						

456

457 **Model biases versus environmental constraints**

458 Overall, the theoretical model for χ showed a significant positive bias with increasing z
 459 (decreasing P_{atm}) mainly due to two sites ($p < 0.001$; Fig. 5c) but no bias related to T_g , $\ln D_g$ or
 460 c_a were detected (Figs 5a-b). Nevertheless, there were significant biases with changing T_g , \ln
 461 D_g or c_a at some individual sites (Figs 5a-b) but the magnitudes and signs of these biases varied
 462 among sites.

463



464

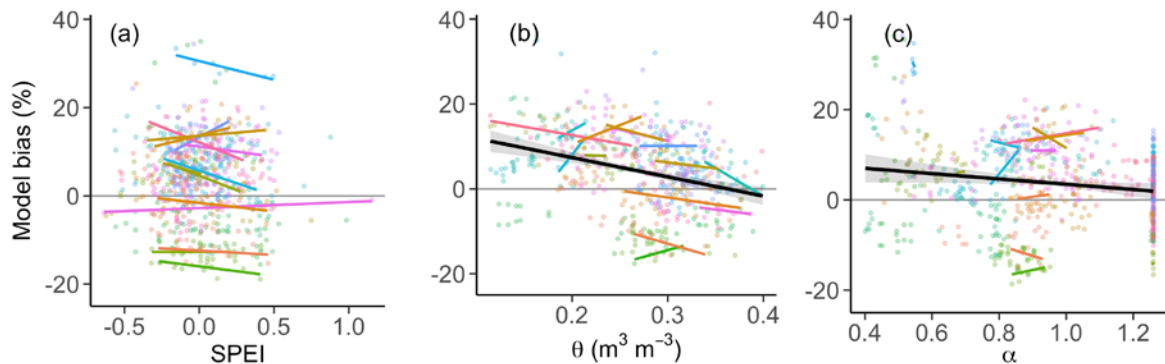
465 **Fig. 5** Partial residual of the model bias (%) in χ predicted by the theoretical model plotted
 466 against growing-season mean daytime climate variables (a, temperature T_g ; b, natural log-
 467 transformed vapour pressure deficit D_g), c, partial pressure of CO_2 corrected for elevation effect
 468 (c_a) and d, elevation (z) during 1951-2014. The solid black line is the regression line for all
 469 sites. The grey-shaded area represents the 95% confidence interval for the regression line. Only
 470 significant trends ($p < 0.05$) are shown. Colours are as in Fig. 4, i.e. representing the different
 471 sites.

472

473

474 Including one of the indices of soil water availability, i.e. θ or α , as additional driver of logit
 475 χ_{iso} in the linear regression model slightly improved the model fits (lower AIC and BIC,
 476 significant ANOVA test, $p < 0.05$) but both the dependencies of logit χ_{iso} on z and on c_a were
 477 then no longer significant (Table S2b). The model showed a significant negative bias with
 478 increasing θ and α (Fig. 6b-c), indicating an overestimation of χ at low soil-moisture sites and
 479 underestimation of χ at high soil-moisture sites at least over the 1979-2014 period. Note that
 480 model biases related to these additional drivers diverged from the general responses at some
 481 individual sites.

482



483

484 **Fig. 6** Partial residual plots of the model bias (%) in χ predicted by the theoretical model plotted
485 against growing-season average water availability or drought indices over 1979-2014 (a,
486 Standardized Precipitation-Evapotranspiration Index, SPEI; b, surface soil moisture content, θ ;
487 c, Priestley-Taylor coefficient, α) (see Table S2b). The solid colour lines indicate the modelled
488 response from the multiple linear regression models for each site, while the solid black lines
489 are those for all sites combined. The grey-shaded area represents the 95% confidence interval
490 for the regression line. Only significant trends at 95% ($p < 0.05$) are shown. Colours are as in
491 Fig. 5, i.e. representing the different sites.

492

493 **4. Discussion**

494 The aim of our study was to evaluate long-term values and trends of χ as predicted by the least-
495 cost hypothesis against a large network of stable carbon isotope-derived χ series from tree
496 rings. Our results are compelling as they demonstrate that despite uncertainties related to the
497 use of tree-ring $\delta^{13}\text{C}$ data as proxy of leaf-gas exchanges (see also Text S4), the model predicted
498 39% of the variance in χ across sites and years. However, only 8% of the variance in χ trends
499 across years was explained by the model, in part due to the larger site-to-site variability in χ
500 trends reported in the tree-ring dataset compared to the predictions. In the following sections,
501 we address both the skills and limitations of the model for predicting plant stomatal and
502 photosynthetic adjustments to environmental conditions. We also discuss potential additional
503 drivers of χ to consider in future studies.

504

505 **Main drivers influencing χ and biases in the model**

506 Rising T_g increases photosynthetic costs by increasing the Michaelis constant of Rubisco (K),
507 whilst reducing water transport costs due to the reduced viscosity of water (η^*). Both effects
508 combined with the increase in the photorespiratory compensation point (Γ^*) with higher T_g are
509 expected to lead to higher ξ (Eqn 4). However, D_g tends to increase with rising T_g , so the effect
510 of temperature on χ , being influenced in opposite ways by ξ and D_g (Wang *et al.*, 2017a), is
511 not straightforward to predict. Increasing D_g tends to increase the water transport required per
512 mole of carbon fixed, and thus the transpiration costs, leading to lower χ . Decreasing P_{atm}
513 decreases K , due to the reduced partial pressure of O_2 , thereby increasing the affinity of Rubisco
514 for CO_2 and reducing the carboxylation capacity required per mole of carbon fixed. At the same
515 time, (all else equal) the actual vapour pressure declines while the saturated vapour pressure

516 remains constant, implying an increase in D_g . Thus, as P_{atm} decreases (z increases), both effects
517 preferentially enhance Rubisco capacity relative to water transport capacity, favouring a lower
518 χ (Körner & Diemer, 1987; Körner *et al.*, 1991; Terashima *et al.*, 1995; Wang *et al.*, 2017a).
519 Finally, elevated c_a increases photosynthesis by increasing the carboxylation rate, while also
520 increasing the transpiration efficiency of plants via a decrease in stomatal conductance. As a
521 result, the direct effect of c_a on χ is difficult to assess at first glance.

522 In general, rising T_g tended to cause an increase of $\logit \chi_{\text{iso}}$, suggesting that the temperature
523 dependencies of K , Γ^* and η^* had a stronger impact on χ than that of D_g (Fig. 5a). As expected,
524 lower χ_{iso} values were observed with increasing D_g and z (Fig. 5b-c), consistent with previous
525 studies (Körner & Diemer, 1987; Körner, Farquhar, & Wong, 1991; Zhu, Siegwolf, Durka, &
526 Körner, 2010). Overall, the slight decrease in $\logit \chi_{\text{iso}}$ with rising c_a implies that c_i increases
527 less than proportionally to increase in c_a . The stronger unique effects of T_g and D_g relative to
528 P_{atm} and c_a on $\logit \chi_{\text{iso}}$ (Table 1) suggests that both T_g and D_g are the dominant drivers of
529 change in χ at many sites. The apparently divergent responses (relative to the general pattern)
530 of $\logit \chi_{\text{iso}}$ to T_g , D_g and c_a at some sites may be indicative of site-specific characteristics not
531 included in the model that also contributed to changes in χ_{iso} . It is also plausible that both T_g
532 and D_g data inferred from the 0.5° resolution CRU dataset, or even the c_a data mainly derived
533 from the Mauna Loa Observatory (Hawaii), were not fully capturing microclimatic differences
534 between or within sites.

535 The environmental dependencies of χ were for the most part captured correctly by the
536 theoretical model (Table 1). Nonetheless, the model tended to underestimate the negative
537 impact of decreasing P_{atm} (increasing z) on χ values (Table 1 and Fig. 6c), suggesting that the
538 observational data were more sensitive to lower P_{atm} (higher z) than predicted by the theory.
539 The positive bias in predicted χ at high-elevation sites was mainly due to two ENF sites both
540 located in the mountains of Kashmir (Table S1; Treydte *et al.*, 2009) and thus could also be an
541 artefact of site selection. These sites were characterised by the lowest mean T_g and D_g values
542 and wettest conditions in the network for the sites located above 2.5 km. It is thus plausible
543 that the combined effects of relatively low T_g and low D_g on χ have dampened the negative
544 effect of low P_{atm} (high z) on predicted χ values. It is worth noting that the dependency of χ on
545 z depends on the relative humidity and the actual vapour pressure. As a result, the predicted
546 coefficient for the elevational dependency of χ in the linear regression (here -0.040 ; Table 1)
547 is not expected to be of same magnitude as the theoretical coefficient estimated under standard

548 conditions ($T = 25^\circ\text{C}$ and relative humidity = 50%) in the former study (i.e. Wang *et al.*, 2017b;
549 -0.0815 , see Text S5).

550

551 **Other potential controls on χ**

552 The large variability in the magnitude of χ_{iso} trends among sites (Fig. 3) and the different
553 dependences of χ_{iso} to the environmental constraints at some sites (Fig. 5) suggest that other
554 controls on χ not captured by the model are operating and may explain part of the remaining
555 variance in χ_{iso} that was mostly assigned to random effects by the linear mixed-effects models
556 (Table S2a). For instance, the least-cost hypothesis considers the influence of atmospheric
557 demand for water on χ but does not predict how dry soils further influence χ (Verhoef & Egea,
558 2014; Rogers *et al.*, 2017). Here we found that, independent of the individual effects of T_g , D_g ,
559 c_a and z on χ , the model tended to underestimate χ values at high soil moisture and to
560 overestimate χ values at low soil moisture (Fig. 7b-c). In a meta-analysis of drying
561 experiments, Zhou *et al.* (2013) demonstrated that the parameter g_1 of the Medlyn *et al.* (2011)
562 model, based on the Cowan-Farquhar optimality hypothesis – mathematically equivalent to ξ
563 in the least-cost model – is reduced by low soil moisture, and that this occurs at a less negative
564 pre-dawn water potential than the decline in V_{cmax} that occurs in very dry soils. Thus, under
565 drying conditions with reduced soil water availability, χ is expected to decrease via a reduction
566 of ξ . Nonetheless, because D_g and soil moisture are tightly coupled at weekly to monthly
567 timescales (Sulman *et al.*, 2016; Gentine *et al.*, 2019), their relative contributions on changes
568 in χ may be difficult to disentangle (Buckley, 2017; Zhou *et al.*, 2019; Yi *et al.*, 2019),
569 complicating the inclusion of soil water limitation in the framework of the least-cost optimality
570 hypothesis. Recent research testing empirical parameterizations of the effect of soil moisture
571 on gross primary production suggests that the value for β , held constant here, should in fact
572 decline with decreasing soil moisture content (Stocker *et al.*, 2018, 2019b). Further research at
573 sites with different soil water availability and different evaporative demand should help in
574 implementing soil moisture effect in the model through a theoretically motivated reduction of
575 β .

576 Some studies have suggested that increases in leaf N content with fossil fuel combustion and
577 agricultural emissions (Galloway *et al.*, 2008) might stimulate photosynthetic capacity (Walker
578 *et al.*, 2014) and increase stomatal conductance, resulting in changes in $\Delta^{13}\text{C}$ and χ . Based on
579 experiments where N and S fertilizers were applied directly to tree canopies, Guerrieri *et al.*

580 (2011) found strong effects of both on $\Delta^{13}\text{C}$ and χ , with the magnitude of changes related to
581 the element and the time since application or cessation. Their results generally agreed with
582 previous work demonstrating that the effect of N fertilization on tree-ring $\Delta^{13}\text{C}$ is short-lived
583 (Brooks & Coulombe, 2009). Nevertheless, the causal mechanisms underlying $\Delta^{13}\text{C}$ responses
584 to both climate and N deposition are not well established (Leonardi *et al.*, 2012). Based on an
585 observational global dataset of V_{cmax} , Smith *et al.* (2019) showed that the dependence of V_{cmax}
586 on leaf N was overestimated in vegetation models, as also suggested by Rogers (2014) – and
587 that V_{cmax} can be predicted well from T_g , D_g , z and light availability alone. These findings
588 suggest that leaf N deposition is not a primary driver of photosynthetic capacity, but rather that
589 the photosynthetic demand itself constrains leaf N content (Dong *et al.*, 2017). Thus, even
590 though changes in leaf N concentrations accompanying changes in V_{cmax} can affect both $\Delta^{13}\text{C}$
591 and χ , we suggest that the environmental drivers of such variations are implicitly included in
592 the least-cost model.

593 Even though some processes influencing χ may be missing, our compilation of 103 tree-ring
594 $\delta^{13}\text{C}$ records supports the theoretical optimal responses of χ to a combination of T_g , D_g , P_{atm}
595 and c_a over the period 1951–2014 as predicted by the least-cost hypothesis (Prentice *et al.*,
596 2014; Wang *et al.*, 2017b). Crucially, the theory predicts χ to be only slightly dependent on c_a ,
597 implying that rising c_a leads to a quasi-proportional increase in c_i and an increase in the
598 biochemical rate of carbon uptake (Farquhar *et al.*, 1980). As c_a rises, the ratio of Γ^* to c_a
599 declines and the average responses of χ to c_a converges to zero (Eqn 4). This response is
600 supported by experimental studies showing no change or a small decrease in χ , on average,
601 with sustained CO_2 enrichment (Ainsworth & Long, 2005), and by historical studies (Keeling
602 *et al.*, 2017; Schubert & Jahren, 2018). This response, however, also contrasts with several
603 studies using leaf and wood $\delta^{13}\text{C}$ measurements from CO_2 enrichment experiments and/or
604 palaeorecords apparently showing an increase of χ with rising c_a at c_a levels ranging from 200
605 to 600 ppm (Voelker *et al.*, 2016; Hare *et al.*, 2018), or even a large decrease of χ with sustained
606 CO_2 enrichment (Battipaglia *et al.*, 2013). It is worth noting that these studies did not include
607 the photorespiration term in the discrimination model. The apparent strong influence of rising
608 c_a on χ in these studies might be an artefact caused by disregarding this effect, as was also
609 indicated by Schubert & Jahren (2018) and Lavergne *et al.* (2019). Our analysis of partial
610 residuals of logit χ_{iso} suggests that, across geographically and phylogenetically diverse trees,

611 the average response of χ_{iso} to c_a is weak (Table 1 and Fig. 5) – as predicted by the least-cost
612 hypothesis.

613 Our results have strong implications for the understanding of the coupled terrestrial carbon and
614 water cycles, because they indicate that the increase in intrinsic water-use efficiency (iWUE)
615 expected with rising atmospheric CO₂ can be offset by increasing T_g (or, potentially, by
616 decreasing D_g and/or increasing soil moisture availability). Also, for the same increase in
617 atmospheric CO₂, iWUE may increase with decreasing P_{atm} (increasing z). Our research
618 complements recent attempts to quantify the relative contributions of environmental drivers to
619 changes in plant water use (Frank *et al.*, 2015; Dekker *et al.*, 2016; Adams *et al.*, 2019) by
620 highlighting eco-evolutionary optimality mechanisms underlying these changes.

621 Current vegetation and land-surface models suffer from large uncertainties, mainly due to
622 incomplete or inaccurate representations of the fundamental processes governing not only leaf-
623 level gas exchange (Raczka *et al.*, 2018), but also competition, carbon allocation, demography
624 and responses to disturbances such as wildfires and insects attacks. Improving the
625 representation of ecophysiological responses to the environment is only part of a much bigger
626 problem with current terrestrial models. It is a central part nonetheless, and our research
627 suggests a way forward – based on optimality theory – for the representation of the coupled
628 terrestrial carbon and water cycles in next-generation Earth System models.

629

630 **Acknowledgments**

631 We thank the three anonymous reviewers for their useful and constructive comments and
632 suggestions. We acknowledge all data providers and the many contributors who helped
633 produce the dataset analysed here. A.L. was supported by a Postdoctoral Newton International
634 Fellowship (Grant no. NF170082) funded by the Royal Society (UK). I.D-L. received financial
635 support from Fundació La Caixa through the Junior Leader Program
636 (LCF/BQ/LR18/11640004). This work contributes to the AXA Chair Programme in Biosphere
637 and Climate Impacts and the Imperial College initiative on Grand Challenges in Ecosystems
638 and the Environment. The project has also received funding from the European Research
639 Council (ERC) under the European Union's Horizon 2020 Research and Innovation
640 Programme (Grant Agreement No: 787203 REALM).

641

642 **Author contributions**

643 A.L and I.C.P. designed the research. S.V., A.C, H.J.deB., V.D., I.R., I.D-L., E.M-S., G.B.,
644 F.C.M., J.J.C., R.C., Y.F., A.M., C.J.S., R.M.K., J.S.R. and T.E.D. provided tree-ring carbon
645 isotopic data. A.L. compiled and analysed the data. A.L. and K.J.B. computed the linear mixed-
646 effect models. A.L. wrote the paper with input and revisions from all co-authors.

647

648 **Code and data availability**

649 The implementation of the model in R is available via the R package `rpmode`
650 (<https://github.com/stineb/rpmode>; Stocker *et al.*, 2019a). The R code used for all the
651 numerical analyses presented here is available through
652 https://github.com/Alielav/NP_Lavergneetal2019. The isotope-derived and predicted χ data
653 over the 1951-2014 period are provided in the Supporting Information. Except for data
654 explicitly specified as available upon request in Table S1, all the tree-ring $\delta^{13}\text{C}$ data are
655 available in the Supporting Information.

656

657 **References**

658 **Adams MA, Buckley TN, Turnbull TL. 2019.** Rainfall drives variation in rates of change in
659 intrinsic water use efficiency of tropical forests. *Nature Communications* **10**: 1–8.

660 **Ainsworth EA, Long SP. 2005.** What have we learned from 15 years of free-air CO₂
661 enrichment (FACE)? A meta-analytic review of the responses of photosynthesis, canopy
662 properties and plant production to rising CO₂. *New Phytologist* **165**: 351–372.

663 **Akaike H. 1973.** Information theory and an extension of the maximum likelihood principle.
664 In: Second International Symposium on Information Theory. 267–281.

665 **Allen RG, Pereira LS, Raes D, Smith M. 1998.** Crop evapotranspiration - Guidelines for
666 computing crop water requirements - FAO Irrigation and drainage paper 56. *Irrigation and*
667 *Drainage*: 1–15.

668 **Badeck FW, Tcherkez G, Nogués S, Piel C, Ghashghaie J. 2005.** Post-photosynthetic
669 fractionation of stable carbon isotopes between plant organs - A widespread phenomenon.
670 *Rapid Communications in Mass Spectrometry* **19**: 1381–1391.

671 **Ballantyne AP, Andres R, Houghton R, Stocker BD, Wanninkhof R, Anderegg W,**
672 **Cooper LA, DeGrandpre M, Tans PP, Miller JB, et al. 2015.** Audit of the global carbon

673 budget: Estimate errors and their impact on uptake uncertainty. *Biogeosciences* **12**: 2565–
674 2584.

675 **Ballantyne AP, Miller JB, Tans PP. 2010.** Apparent seasonal cycle in isotopic
676 discrimination of carbon in the atmosphere and biosphere due to vapor pressure deficit.
677 *Global Biogeochemical Cycles* **24**: 1–16.

678 **Bates D, Mächler M, Bolker B, Walker S. 2015.** Fitting linear mixed-effects models using
679 lme4. *Journal of Statistical Software* **67**: 1–48.

680 **Battipaglia G, Saurer M, Cherubini P, Calfapietra C, Mccarthy HR, Norby RJ,
681 Francesca Cotrufo M. 2013.** Elevated CO₂ increases tree-level intrinsic water use
682 efficiency: Insights from carbon and oxygen isotope analyses in tree rings across three forest
683 FACE sites. *New Phytologist* **197**: 544–554.

684 **Beguéría S, Vicente-Serrano SM, Angulo-Martínez M. 2010.** A multiscalar global drought
685 dataset: The SPEI base: A new gridded product for the analysis of drought variability and
686 impacts. *Bulletin of the American Meteorological Society* **91**: 1351–1356.

687 **Bernacchi CJ, Singsaas EL, Pimentel C, Portis Jr AR, Long SP. 2001.** Improved
688 temperature response functions for models of Rubisco-limited photosynthesis. *Plant, Cell
689 and Environment* **24**: 253–259.

690 **Bloomfield KJ, Prentice IC, Cernusak LA, Eamus D, Medlyn BE, Wright IJ, Boer MM,
691 Cale P, Cleverly J, Egerton JJG, et al. 2019.** The validity of optimal leaf traits modelled on
692 environmental conditions. *New Phytologist* **221**: 1409–1423.

693 **Bolker BM, Brooks ME, Clark CJ, Geange SW, Poulsen JR, Stevens MHH, White JSS.
694 2009.** Generalized linear mixed models: a practical guide for ecology and evolution. *Trends
695 in Ecology and Evolution* **24**: 127–135.

696 **Bowling DR, Pataki DE, Randerson JT. 2008.** Carbon isotopes in terrestrial ecosystem
697 pools and CO₂ fluxes. *New Phytologist* **178**: 24–40.

698 **Brooks JR, Coulombe R. 2009.** Physiological responses to fertilization recorded in tree
699 rings: isotopic lessons from a long-term fertilization trial. *Ecological Applications* **19**: 1044–
700 1060.

701 **Buckley TN. 2017.** Modeling Stomatal Conductance. *Plant Physiology* **174**: 572–582.

702 **Buckley TN, Schymanski SJ. 2014.** Stomatal optimisation in relation to atmospheric CO₂.
703 *New Phytologist* **201**: 372–377.

704 **von Caemmerer S, Evans JR. 2015.** Temperature responses of mesophyll conductance
705 differ greatly between species. *Plant, Cell and Environment* **38**: 629–637.

706 **Ciais P, Sabine C, Bala G, Bopp L, Brovkin V, Canadell J, Chhabra A, DeFries R,**

707 **Galloway J, Heimann M, et al. 2013.** 2013: Carbon and other biogeochemical cycles.
708 *Climate Change 2013: The Physical Science Basis. Contribution of Working Group I to the*
709 *Fifth Assessment Report of the Intergovernmental Panel on Climate Change.*: 465–570.

710 **Cowan IR, Farquhar GD. 1977.** Stomatal function in relation to leaf metabolism and
711 environment. *Symp Soc Exp Biol.* **31**: 471–505.

712 **Craig H. 1953.** The geochemistry of the stable carbon isotopes. *Geochimica et*
713 *Cosmochimica Acta* **3**: 53–92.

714 **Davis TW, Prentice IC, Stocker BD, Thomas RT, Whitley RJ, Wang H, Evans BJ,**
715 **Gallego-Sala A V., Sykes MT, Cramer W. 2017.** Simple process-led algorithms for
716 simulating habitats (SPLASH v.1.0): Robust indices of radiation, evapotranspiration and
717 plant-available moisture. *Geoscientific Model Development* **10**: 689–708.

718 **Dekker SC, Groenendijk M, Booth BBB, Huntingford C, Cox PM. 2016.** Spatial and
719 temporal variations in plant water-use efficiency inferred from tree-ring, eddy covariance and
720 atmospheric observations. *Earth System Dynamics* **7**: 525–533.

721 **Dewar R, Mauraanen A, Mäkelä A, Hölttä T, Medlyn B, Vesala T. 2018.** New insights
722 into the covariation of stomatal, mesophyll and hydraulic conductances from optimization
723 models incorporating nonstomatal limitations to photosynthesis. *New Phytologist* **217**: 571–
724 585.

725 **Dong N, Prentice IC, Evans BJ, Caddy-Retalic S, Lowe AJ, Wright IJ. 2017.** Leaf
726 nitrogen from first principles: field evidence for adaptive variation with climate.
727 *Biogeosciences* **14**: 481–495.

728 **Dorado-Liñán I, Piovesan G, Martínez-Sancho E, Gea-Izquierdo G, Zang C, Cañellas I,**
729 **Castagneri D, Di Filippo A, Gutiérrez E, Ewald J, et al. 2019.** Geographical adaptation
730 prevails over species-specific determinism in trees' vulnerability to climate change at
731 Mediterranean rear-edge forests. *Global Change Biology* **25**: 1296–1314.

732 **Dorigo W, Wagner W, Albergel C, Albrecht F, Balsamo G, Brocca L, Chung D, Ertl M,**
733 **Forkel M, Gruber A, et al. 2017.** ESA CCI Soil Moisture for improved Earth system
734 understanding: State-of-the art and future directions. *Remote Sensing of Environment* **203**:
735 185–215.

736 **Ehleringer JR, Hall AE, Farquhar GD. 1993.** Water use in relation to productivity. In:
737 Ehleringer JR, Hall A, Farquhar GD, eds. Stable isotopes and plant carbon-water relations.
738 Academic Press Inc., San Diego, Calif, 155–172.

739 **Evans JR, Von Caemmerer S. 2013.** Temperature response of carbon isotope
740 discrimination and mesophyll conductance in tobacco. *Plant, Cell and Environment* **36**: 745–

741 756.

742 **Eyring V, Bony S, Meehl GA, Senior C, Stevens B, Stouffer RJ, Taylor KE. 2016.**
743 Overview of the Coupled Model Intercomparison Project Phase 6 (CMIP6) experimental
744 design and organisation. *Geoscientific Model Development Discussions* **8**: 10539–10583.

745 **Farquhar GD, von Caemmerer S, Berry JA. 1980.** A biochemical model of photosynthetic
746 CO₂ assimilation in leaves of C₃ species. *Planta* **149**: 78–90.

747 **Farquhar GD, O’Leary MH, Berry JA. 1982.** On the relationship between carbon isotope
748 discrimination and the intercellular carbon dioxide concentration in leaves. *Australian*
749 *Journal of Plant Physiology* **9**: 121–137.

750 **Flexas J, Ribas-Carbó M, Diaz-Espejo A, Galmés J, Medrano H. 2008.** Mesophyll
751 conductance to CO₂: Current knowledge and future prospects. *Plant, Cell and Environment*
752 **31**: 602–621.

753 **Fox J, Weisberg S, Friendly M, Hong J, Andersen R, Firth D, Steve T. 2018.** R package
754 ‘effects’: effect displays for linear, generalized linear, and other models.

755 **Frank DC, Poulter B, Saurer M, Esper J, Huntingford C, Helle G, Treydte K,**
756 **Zimmermann NE, Schleser GH, Ahlström A, et al. 2015.** Water-use efficiency and
757 transpiration across European forests during the Anthropocene. *Nature Climate Change* **5**:
758 579–583.

759 **Fürstenau Togashi H, Colin Prentice I, Atkin OK, Macfarlane C, Prober SM,**
760 **Bloomfield KJ, Evans BJ. 2018.** Thermal acclimation of leaf photosynthetic traits in an
761 evergreen woodland, consistent with the coordination hypothesis. *Biogeosciences* **15**: 3461–
762 3474.

763 **Galloway JN, Townsend AR, Erisman JW, Bekunda M, Cai Z, Freney JR, Martinelli**
764 **LA, Seitzinger SP, Sutton MA. 2008.** Transformation of the nitrogen cycle: Recent trends,
765 questions, and potential solutions. *Science* **320**: 889–892.

766 **Gentine P, Green J, Guerin M, Humphrey V, Seneviratne SI, Zhang Y, Zhou S. 2019.**
767 Coupling between the terrestrial carbon and water cycles - a review. *Environmental Research*
768 *Letters*: 1–18.

769 **Gessler A, Ferrio JP, Hommel R, Treydte K, Werner RA, Monson RK. 2014.** Stable
770 isotopes in tree rings: towards a mechanistic understanding of isotope fractionation and
771 mixing processes from the leaves to the wood. *Tree Physiology* **34**: 796–818.

772 **Ghashghaie J, Badeck F-W, Lanigan G, Nogués S, Tcherkez G, Deléens E, Cornic G,**
773 **Griffiths H. 2003.** Carbon isotope fractionation during dark respiration and photorespiration
774 in C₃ plants. *Phytochemistry Reviews* **2**: 145–161.

775 **Gimeno TE, Saavedra N, Ogée J, Medlyn BE, Wingate L. 2019.** A novel optimization
776 approach incorporating non-stomatal limitations predicts stomatal behaviour in species from
777 six plant functional types. *Journal of Experimental Botany* **70**: 1639–1651.

778 **Givnish TJ. 1986.** Optimal stomatal conductance, allocation of energy between leaves and
779 roots, and the marginal cost of transpiration. In: *On the Economy of Plant Form and*
780 *Function*. Cambridge: Cambridge University Press, 171–213.

781 **Graven H, Allison CE, Etheridge DM, Hammer S, Keeling RF, Levin I, Meijer HAJ,**
782 **Rubino M, Tans PP, Trudinger CM, et al. 2017.** Compiled records of carbon isotopes in
783 atmospheric CO₂ for historical simulations in CMIP6. *Geoscientific Model Development* **10**:
784 4405–4417.

785 **Green JK, Seneviratne SI, Berg AM, Findell KL, Hagemann S, Lawrence DM, Gentine**
786 **P. 2019.** Large influence of soil moisture on long-term terrestrial carbon uptake. *Nature* **565**:
787 476–479.

788 **Guerrieri R, Mencuccini M, Sheppard LJ, Saurer M, Perks MP, Levy P, Sutton MA,**
789 **Borghetti M, Grace J. 2011.** The legacy of enhanced N and S deposition as revealed by the
790 combined analysis of $\delta^{13}\text{C}$, $\delta^{18}\text{O}$ and $\delta^{15}\text{N}$ in tree rings. *Global Change Biology* **17**: 1946–
791 1962.

792 **Hare VJ, Loftus E, Jeffrey A, Ramsey CB. 2018.** Atmospheric CO₂ effect on stable carbon
793 isotope composition of terrestrial fossil archives. *Nature Communications* **9**: 252.

794 **Harris I, Jones PD, Osborn TJ, Lister DH. 2014.** Updated high-resolution grids of monthly
795 climatic observations - the CRU TS3.10 Dataset. *International Journal of Climatology* **34**:
796 623–642.

797 **Huber ML, Perkins RA, Laesecke A, Friend DG, Sengers JV, Assael MJ, Metaxa IN,**
798 **Vogel E, Mares R, Miyagawa K. 2009.** New international formulation for the viscosity of
799 H₂O. *J. Phys. Chem. Ref. Data* **38**: 101–125.

800 **Humphrey V, Zscheischler J, Ciais P, Gudmundsson L, Sitch S, Seneviratne SI. 2018.**
801 Sensitivity of atmospheric CO₂ growth rate to observed changes in terrestrial water storage.
802 *Nature* **560**: 628–631.

803 **Jones HG. 2013.** *Plants and Microclimate*. Cambridge: Cambridge University Press.

804 **Jones CD, Arora V, Friedlingstein P, Bopp L, Brovkin V, Dunne J, Graven H, Hoffman**
805 **F, Ilyina T, John JG, et al. 2016.** C4MIP-The Coupled Climate-Carbon Cycle Model
806 Intercomparison Project: experimental protocol for CMIP6. *Geoscientific Model*
807 *Development* **9**: 2853–2880.

808 **Katul G, Manzoni S, Palmroth S, Oren R. 2010.** A stomatal optimization theory to

809 describe the effects of atmospheric CO₂ on leaf photosynthesis and transpiration. *Annals of*
810 *Botany* **105**: 431–442.

811 **De Kauwe MG, Medlyn BE, Zaehle S, Walker AP, Dietze MC, Hickler T, Jain AK, Luo**
812 **Y, Parton WJ, Prentice IC, et al. 2013.** Forest water use and water use efficiency at
813 elevated CO₂: A model-data intercomparison at two contrasting temperate forest FACE sites.
814 *Global Change Biology* **19**: 1759–1779.

815 **De Kauwe MG, Medlyn BE, Zaehle S, Walker AP, Dietze MC, Wang Y-P, Luo Y, Jain**
816 **AK, El-Masri B, Hickler T, et al. 2014.** Where does the carbon go? A model-data
817 intercomparison of vegetation carbon allocation and turnover processes at two temperate
818 forest free-air CO₂ enrichment sites. *New Phytologist* **203**: 883–899.

819 **Keeling RF, Graven HD, Welp LR, Resplandy L, Bi J, Piper SC, Sun Y, Bollenbacher**
820 **A, Meijer HAJ. 2017.** Atmospheric evidence for a global secular increase in carbon isotopic
821 discrimination of land photosynthesis. *Proceedings of the National Academy of Sciences* **114**:
822 10361–10366.

823 **Keller KM, Lienert S, Bozbiyik A, Stocker TF, Churakova Sidorova O V., Frank DC,**
824 **Klesse S, Koven CD, Leuenberger M, Riley WJ, et al. 2017.** 20th century changes in
825 carbon isotopes and water-use efficiency: Tree-ring-based evaluation of the CLM4.5 and
826 LPX-Bern models. *Biogeosciences* **14**: 2641–2673.

827 **Knorr W, Prentice IC, House JI, Holland EA. 2005.** Long-term sensitivity of soil carbon
828 turnover to warming. *Nature* **433**: 298–301.

829 **Körner C, Diemer M. 1987.** In situ photosynthetic responses to light, temperature and
830 carbon dioxide in herbaceous plants from low and high altitude. *Functional Ecology* **1**: 179–
831 194.

832 **Körner C, Farquhar GD, Wong SC. 1991.** Carbon isotope discrimination by plants follows
833 latitudinal and altitudinal trends. *Oecologia* **88**: 30–40.

834 **Lavergne A, Graven H, De Kauwe MG, Keenan TF, Medlyn BE, Prentice IC. 2019.**
835 Observed and modelled historical trends in the water-use efficiency of plants and ecosystems.
836 *Global Change Biology* **25**: 2242–2257.

837 **Leonardi S, Gentilesca T, Guerrieri R, Ripullone F, Magnani F, Mencuccini M, Noiye T**
838 **V., Borghetti M. 2012.** Assessing the effects of nitrogen deposition and climate on carbon
839 isotope discrimination and intrinsic water-use efficiency of angiosperm and conifer trees
840 under rising CO₂ conditions. *Global Change Biology* **18**: 2925–2944.

841 **Li J, Wang G, Mayes MA, Allison SD, Frey SD, Shi Z, Hu X-M, Luo Y, Melillo JM.**
842 **2018.** Reduced carbon use efficiency and increased microbial turnover with soil warming.

843 *Global Change Biology* **25**: 900–910.

844 **Lüdecke D, Makowski D, Waggoner P. 2019.** performance: Assessment of Regression
845 Models Performance. R package version 0.2.0.9000.

846 **Manzoni S, Vico G, Palmroth S, Porporato A, Katul G. 2013.** Optimization of stomatal
847 conductance for maximum carbon gain under dynamic soil moisture. *Advances in Water*
848 *Resources* **62**: 90–105.

849 **Martínez-Sancho E, Dorado-Liñán I, Gutiérrez Merino E, Matiu M, Helle G, Heinrich**
850 **I, Menzel A. 2018.** Increased water-use efficiency translates into contrasting growth patterns
851 of Scots pine and sessile oak at their southern distribution limits. *Global Change Biology* **24**:
852 1012–1028.

853 **Medlyn BE, Duursma RA, Eamus D, Ellsworth DS, Prentice IC, Barton CVM, Crous**
854 **KY, De Angelis P, Freeman M, Wingate L. 2011.** Reconciling the optimal and empirical
855 approaches to modelling stomatal conductance. *Global Change Biology* **17**: 2134–2144.

856 **Medlyn BE, Duursma RA, De Kauwe MG, Prentice IC. 2013.** The optimal stomatal
857 response to atmospheric CO₂ concentration: Alternative solutions, alternative interpretations.
858 *Agricultural and Forest Meteorology* **182–183**: 200–203.

859 **Moldover MR, Trusler JPM, Edwards TJ, Mehl JB, Davis RS. 1988.** Measurement of the
860 universal gas constant R using a spherical acoustic resonator. *Journal of Research of the*
861 *National Bureau of Standards* **93**: 85–114.

862 **Nimon K, Oswald F, Roberts JK. 2013.** yhat: Interpreting Regression Effects. R package
863 version 2.0-0.

864 **Park R, Epstein S. 1960.** Carbon isotope fractionation during photosynthesis. *Geochimica et*
865 *Cosmochimica Acta* **21**: 110–226.

866 **Peters W, van der Velde IR, van Schaik E, Miller JB, Ciais P, Duarte HF, van der**
867 **Laan-Luijkx IT, van der Molen MK, Scholze M, Schaefer K, et al. 2018.** Increased water-
868 use efficiency and reduced CO₂ uptake by plants during droughts at a continental scale.
869 *Nature Geoscience* **11**: 744–748.

870 **Pohlert T. 2018.** trend: non-parametric trend tests and change-point detection.

871 **Prentice IC, Dong N, Gleason SM, Maire V, Wright IJ. 2014.** Balancing the costs of
872 carbon gain and water transport: Testing a new theoretical framework for plant functional
873 ecology. *Ecology Letters* **17**: 82–91.

874 **Le Quéré C, Andrew RM, Friedlingstein P, Sitch S, Hauck J, Pongratz J, Pickers PA,**
875 **Korsbakken JJ, Peters GP, Canadell JG, et al. 2018.** Global Carbon Budget 2018. *Earth*
876 *System Science Data* **10**: 2141–2194.

877 **R Core Team, R Development Core Team R. 2018.** R: A language and environment for
878 statistical computing. (RDC Team, Ed.). *R Foundation for Statistical Computing* **1**: 409.

879 **Raczka B, Dietze MC, Serbin SP, Davis KJ. 2018.** What limits predictive certainty of long-
880 term carbon uptake? *Journal of Geophysical Research: Biogeosciences* **123**: 3570–3588.

881 **Raczka B, Duarte HF, Koven CD, Ricciuto D, Thornton PE, Lin JC, Bowling DR. 2016.**
882 An observational constraint on stomatal function in forests: Evaluating coupled carbon and
883 water vapor exchange with carbon isotopes in the Community Land Model (CLM4.5).
884 *Biogeosciences* **13**: 5183–5204.

885 **Reich PB, Hobbie SE. 2013.** Decade-long soil nitrogen constraint on the CO₂ fertilization of
886 plant biomass. *Nature Climate Change* **3**: 278–282.

887 **Reich PB, Hobbie SE, Lee T, Ellsworth DS, West JB, Tilman D, Knops JMH, Naeem S,
888 Trost J. 2006.** Nitrogen limitation constrains sustainability of ecosystem response to CO₂.
889 *Nature* **440**: 922–925.

890 **Rogers A. 2014.** The use and misuse of $V_{c,max}$ in Earth System Models. *Photosynthesis*
891 *Research* **119**: 15–29.

892 **Rogers A, Medlyn BE, Dukes JS, Bonan G, von Caemmerer S, Dietze MC, Kattge J,
893 Leakey ADB, Mercado LM, Niinemets Ü, et al. 2017.** A roadmap for improving the
894 representation of photosynthesis in Earth system models. *New Phytologist* **213**: 22–42.

895 **Saurer M, Spahni R, Frank DC, Joos F, Leuenberger M, Loader NJ, McCarroll D,
896 Gagen M, Poulter B, Siegwolf RTW, et al. 2014.** Spatial variability and temporal trends in
897 water-use efficiency of European forests. *Global Change Biology* **20**: 3700–3712.

898 **Schimel D, Stephens BB, Fisher JB. 2015.** Effect of increasing CO₂ on the terrestrial carbon
899 cycle. *Proceedings of the National Academy of Sciences* **112**: 436–441.

900 **Schubert BA, Jahren AH. 2018.** Incorporating the effects of photorespiration into terrestrial
901 paleoclimate reconstruction. *Earth-Science Reviews* **177**: 637–642.

902 **Seibt U, Rajabi A, Griffiths H, Berry JA. 2008.** Carbon isotopes and water use efficiency:
903 Sense and sensitivity. *Oecologia* **155**: 441–454.

904 **Sen PK. 1968.** Estimates of the regression coefficient based on Kendall’s tau. *Journal of the*
905 *American Statistical Association* **63**: 1379–1389.

906 **Smith NG, Keenan TF, Colin Prentice I, Wang H, Wright IJ, Niinemets Ü, Crous KY,
907 Domingues TF, Guerrieri R, Yoko Ishida F, et al. 2019.** Global photosynthetic capacity is
908 optimized to the environment (S Niu, Ed.). *Ecology Letters* **22**: 506–517.

909 **Sperry JS, Venturas MD, Anderegg WRL, Mencuccini M, Mackay DS, Wang Y, Love
910 DM. 2017.** Predicting stomatal responses to the environment from the optimization of

911 photosynthetic gain and hydraulic cost. *Plant Cell and Environment* **40**: 816–830.

912 **Stocker BD, Wang H, Smith NG, Harrison SP, Keenan TF, Sandoval D, Davis T,**
913 **Prentice IC. 2019a.** P-model v1.0: An optimality-based light use efficiency model for
914 simulating ecosystem gross primary production. *Geoscientific Model Development*
915 *Discussions* **37**: 1–59.

916 **Stocker BD, Zscheischler J, Keenan TF, Prentice IC, Peñuelas J, Seneviratne SI. 2018.**
917 Quantifying soil moisture impacts on light use efficiency across biomes. *New Phytologist*
918 **218**: 1430–1449.

919 **Stocker BD, Zscheischler J, Keenan TF, Prentice IC, Seneviratne SI, Peñuelas J. 2019b.**
920 Drought impacts on terrestrial primary production underestimated by satellite monitoring.
921 *Nature Geoscience* **12**: 264–270.

922 **Sulman BN, Roman DT, Yi K, Wang L, Phillips RP, Novick KA. 2016.** High atmospheric
923 demand for water can limit forest carbon uptake and transpiration as severely as dry soil.
924 *Geophysical Research Letters* **43**: 1–8.

925 **Terashima I, Masuzawa T, Ohba H, Yokoi Y. 1995.** Is photosynthesis suppressed at higher
926 elevations due to low CO₂ pressure? *Ecology* **76**: 2663–2668.

927 **Treydte KS, Frank DC, Saurer M, Helle G, Schleser GH, Esper J. 2009.** Impact of
928 climate and CO₂ on a millennium-long tree-ring carbon isotope record. *Geochimica et*
929 *Cosmochimica Acta* **73**: 4635–4647.

930 **Ubierna N, Farquhar GD. 2014.** Advances in measurements and models of photosynthetic
931 carbon isotope discrimination in C₃ plants. *Plant Cell and Environment* **37**: 1494–1498.

932 **Venables WN, Ripley BD. 2002.** *Modern applied statistics with S. Fourth edition.* Springer.

933 **Verhoef A, Egea G. 2014.** Modeling plant transpiration under limited soil water:
934 Comparison of different plant and soil hydraulic parameterizations and preliminary
935 implications for their use in land surface models. *Agricultural and Forest Meteorology* **191**:
936 22–32.

937 **Voelker SL, Brooks JR, Meinzer FC, Anderson R, Bader MK-F, Battipaglia G, Becklin**
938 **KM, Beerling D, Bert D, Betancourt JL, et al. 2016.** A dynamic leaf gas-exchange strategy
939 is conserved in woody plants under changing ambient CO₂: evidence from carbon isotope
940 discrimination in paleo and CO₂ enrichment studies. *Global Change Biology* **22**: 889–902.

941 **Walker AP, Beckerman AP, Gu L, Kattge J, Cernusak LA, Domingues TF, Scales JC,**
942 **Wohlfahrt G, Wullschleger SD, Woodward FI, et al. 2014.** The relationship of leaf
943 photosynthetic traits – V_{cmax} and J_{max} – to leaf nitrogen, leaf phosphorus, and specific leaf
944 area: a meta-analysis and modeling study. *Ecology and Evolution* **4**: 3218–3235.

945 **Wang H, Prentice IC, Davis TW, Keenan TF, Wright IJ, Peng C. 2017a.** Photosynthetic
946 responses to altitude: an explanation based on optimality principles. *New Phytologist* **213**:
947 976–982.

948 **Wang H, Prentice IC, Keenan TF, Davis TW, Wright IJ, Cornwell WK, Evans BJ, Peng**
949 **C. 2017b.** Towards a universal model for carbon dioxide uptake by plants. *Nature Plants* **3**:
950 734–741.

951 **Weedon GP, Balsamo G, Bellouin N, Gomes S, Best MJ, Viterbo P. 2014.** The WFDEI
952 meteorological forcing data set: WATCH Forcing Data methodology applied to ERA-Interim
953 reanalysis data. *Water Resources Research* **50**: 7505–7514.

954 **Wingate L, Seibt U, Maseyk K, Ogée J, Almeida P, Yakir D, Pereira JS, Mencuccini M.**
955 **2008.** Evaporation and carbonic anhydrase activity recorded in oxygen isotope signatures of
956 net CO₂ fluxes from a mediterranean soil. *Global Change Biology* **14**: 2178–2193.

957 **Wolf A, Anderegg WRL, Pacala SW. 2016.** Optimal stomatal behavior with competition
958 for water and risk of hydraulic impairment. *Proceedings of the National Academy of Sciences*
959 **113**: E7222–E7230.

960 **Wright IJ, Reich PB, Westoby M. 2003.** Least-cost input mixtures of water and nitrogen for
961 photosynthesis. *The American Naturalist* **161**: 98–111.

962 **Wullschleger SD, Epstein HE, Box EO, Euskirchen ES, Goswami S, Iversen CM, Kattge**
963 **J, Norby RJ, van Bodegom PM, Xu X. 2014.** Plant functional types in Earth system
964 models: past experiences and future directions for application of dynamic vegetation models
965 in high-latitude ecosystems. *Annals of Botany* **114**: 1–16.

966 **Yi K, Maxwell JT, Wenzel MK, Roman DT, Sauer PE, Phillips RP, Novick KA. 2019.**
967 Linking variation in intrinsic water-use efficiency to isohydricity: a comparison at multiple
968 spatiotemporal scales. *New Phytologist* **221**: 195–208.

969 **Zhao M, Running SW. 2010.** Drought-induced reduction in global terrestrial net primary
970 production from 2000 through 2009. *Science* **329**: 940–943.

971 **Zhou S, Duursma RA, Medlyn BE, Kelly JWG, Prentice IC. 2013.** How should we model
972 plant responses to drought? An analysis of stomatal and non-stomatal responses to water
973 stress. *Agricultural and Forest Meteorology* **182–183**: 204–214.

974 **Zhou S, Zhang Y, Williams AP, Gentine P. 2019.** Projected increases in intensity,
975 frequency, and terrestrial carbon costs of compound drought and aridity events. *Science*
976 *Advances* **5**: 1–9.

977 **Zhu Y, Siegwolf RTW, Durka W, Korner C. 2010.** Phylogenetically balanced evidence for
978 structural and carbon isotope responses in plants along elevational gradients. *Oecologia* **162**:

979 853–863.

980 **Zuur AF, Ieno EN, Walker NJ, Saveliev AA, Smith GM. 2009.** *Mixed Effects Models and*
981 *Extensions in Ecology with R.* New York: Springer.

982